Protein Expression and Purification 177 (2021) 105766

Contents lists available at ScienceDirect

Protein Expression and Purification

journal homepage: www.elsevier.com/locate/yprep

Characterization of a single chain variable fragment of nivolumab that targets PD-1 and blocks PD-L1 binding

Jong Shin [b,1], Paul J. Phelan [a,1,2], Ole Gjoerup [c], William Bachovchin [a], Peter A. Bullock [a,*]

[a] Department of Developmental, Molecular and Chemical Biology, Tufts University School of Medicine, 136 Harrison Avenue, Boston, MA, 02111, USA
[b] Department of Pathology, New York University School of Medicine, 550 First Avenue, New York, NY, 10016, USA
[c] Foundation Medicine, Inc., 150 Second Street, Cambridge, MA, 02141, USA

ARTICLE INFO

Keywords:
Molecular cloning
Purification of an scFv that binds to PD-1
Molecular modeling
Determining the IC50 for the anti-PD-1 scFv
Mechanism by which the anti-PD-1 scFv blocks binding of PD-L1

ABSTRACT

Activated T-cells express Programmed cell Death protein 1 (PD-1), a key immune checkpoint receptor. PD-1 functions primarily in peripheral tissues, where T cells may encounter tumor-derived immunosuppressive ligands. Monoclonal antibodies that disrupt the interaction between T-cell derived PD-1 and immunosuppressive ligands, such as PD-L1, have revolutionized approaches to cancer therapy. For instance, Nivolumab is a monoclonal Ab that targets human PD-1 and has played an important role in immune checkpoint therapy. Herein we report the purification and initial characterization of a ~27 kDa single chain variable fragment (scFv) of Nivolumab that targets human PD-1 and blocks binding by PD-L1. The possibility that the anti-PD-1 scFv can serve as both an anti-tumor agent and as an anti-viral agent is discussed.

Importance: The clinical significance of anti-PD-1 antibodies for treatment of a range of solid tumors is well documented (reviewed in [1–4]). In this report, we describe the results of studies that establish that an anti-PD-1 scFv purified from *E. coli* binds tightly to human PD-1. Furthermore, we demonstrate that upon binding, the anti-PD-1 scFv disrupts the interaction between PD-1 and PD-L1. Thus, the properties of this scFv, including its small size, stability and affinity for human PD-1, suggest that it has the potential to be a useful reagent in subsequent immunotherapeutic, diagnostic and anti-viral applications.

1. Introduction

Activation of "immune checkpoints" is a fundamental event that limits collateral tissue damage during T cell responses to infection (reviewed in Refs. [5–7]). However, activation of immune checkpoints also enables cancer cells to avoid destruction by the human immune system. These negative checkpoints are established when immunosuppressive ligands on cancer cells interact with receptors on immune effector cells [1–3]. As a result of these activated checkpoints, the human immune system does not mount a full attack on many tumors.

One critical form of checkpoint-based inhibition is due to the interaction of the inhibitory receptor Programmed cell Death protein-1 (PD-1), located on the surface of a number of cell types (including activated T cells, T regs, activated B cells and natural killer cells) with ligands such as PD1 ligand 1 (PD-L1) (e.g., Ref. [8–12]; reviewed in Refs. [13]). Normally, the PD-1/PD-L1 interaction plays a critical role in the suppression of $CD8^+$ cytotoxic T cells and related cells of the immune system [2]. As a result, the activity of T cells in inflamed peripheral tissues is regulated and thereby autoimmunity is limited (e.g. Ref. [5]). Unfortunately, many human cancer cells have up-regulated levels of PD-L1 and the PD-1/PD-L1 dependent suppression of immune cells enables cancer cells to escape the immune system and to further proliferate ([14–16]; reviewed in Ref. [16]).

A seminal discovery in the immunotherapy field was that monoclonal antibodies that bind PD-1, and thereby disrupt PD-1's interactions with ligands such as PD-L1, promote T cell proliferation and activation (e.g., Ref. [17]; reviewed in Ref. [4,18,19]). This led to the observation that broad-spectrum antitumor activity can result from antibody-based inhibition of the interaction between PD1 and its ligands (e.g. Refs. [3,5,8,16,20]). Anti-PD1 monoclonal antibodies include Nivolumab

* Corresponding author. Department of Developmental, Molecular and Chemical Biology, Tufts University School of Medicine, 136 Harrison Avenue, S705, Boston, MA, 02111.
E-mail address: Peter.Bullock@tufts.edu (P.A. Bullock).
[1] Current address: Joinn Biologics, 2600 Hilltop Drive, Building L, Richmond, CA, 94,806.
[2] The first two authors contributed equally to this work.

https://doi.org/10.1016/j.pep.2020.105766
Received 3 September 2020; Received in revised form 15 September 2020; Accepted 19 September 2020
Available online 25 September 2020

(OPDIVO [21–25]); Bristol-Myers Squibb) and Keytruda (Pembrolizumab [26]; Merck). It is anticipated that further characterization of these and related molecules will lead to additional strategies to overcome tumor dependent immune checkpoints.

Of interest, single chain derivatives of monoclonal antibodies have been used as surrogates for full-length antibodies ([27,28]; reviewed in Ref. [29,30]). Among the advantages of scFvs is that they have relatively high tumor penetration [31,32] and decreased immunogenicity in humans [33]. Furthermore, they are relatively inexpensive to prepare and are easily modified by genetic manipulations. In view of these and related considerations, we elected to design, purify and characterize an scFv antibody targeting human PD-1.

2. Materials and methods

2.1. Purification of the anti-PD-1 scFv

An inexpensive method for the production of scFv antibodies is via expression in *E. coli* (e.g. Ref. [34]). Therefore, the following steps were taken to clone, express and purify the anti-PD-1 scFv from *E. coli*.

1. Molecular Cloning: The amino-acid sequence for the full-length anti-PD-1 mAb Nivolumab was obtained from the ChEMBL website. Using the Clustal W program, the V_H and V_L regions were identified (Fig. 1A1). DNA encoding the V_H and V_L regions, and a segment of DNA encoding a $(Gly_4S)_3$ repeat used to link the V_H and V_L regions together ((Fig. 1A2 [35]), was purchased from IDT as a gBlock. The anti-PD-1 scFv fragment also contained flanking regions that were homologous to the pLIC plasmid and utilized for plasmid assembly by homologous recombination. Prior to molecular cloning by Gibson Assembly [36], the pLIC-His plasmid was linearized by PCR (the forward primer was 5′CGAGGCTGCTCCCTGGAAATACAGG3′, while the reverse primer was 5′CGAGGCCGGTGCTTTGCAGGATCCG3′). Following fragment assembly, the DNA was transformed into competent *E. coli* cells (NEB5-alpha) and colonies harvested following ampicillin selection. DNA was purified from selected colonies using a Qiagen Miniprep Kit and candidate clones identified by size following agarose gel electrophoresis. The sequence encoding the anti-PD-1 scFv was confirmed by Sanger DNA sequencing. The resulting vector was termed pLIC-His-anti-PD-1. It is noted that the gBlock fragment encoding the anti-PD-1 scFv was cloned into the pLIC plasmid in frame with a 6xHis tag and a TEV protease cleavage site (Fig. 1B1). Thus, following the initial methionine at its N-terminus, the anti-PD1 scFv has residues that form both the 6xHis motif and a TEV protease cleavage site (Fig. 1B2).

2. Expression and Solubilization of the Anti-PD-1 scFv: Plasmid pLIC-His-anti-PD1 was transformed into *E. coli* (BL21 DE3; pLysS). Protein expression was induced at an OD600 of ~0.6 by addition of IPTG (0.1 mM) and the cells were grown for 8 h at 30 °C. The cells were then harvested by centrifugation at 4500 RPM in a Sorvall RC-3B Plus. To initiate the isolation of the scFv, 4 g of cell pellet was re-suspended in 100 mls of Buffer A (50 mM Tris.HCl pH 8.0, 0.3 M NaCl, 2 mM EDTA, 10% glycerol, 1 mM PMSF, 1% Igepal CA-630 and 0.1% β-mercaptoethanol) and the cells lysed by passage two times though an Avestin homogenizer. To remove cell debris and insoluble proteins, the lysate was centrifuged for 30 min at 18,000 rpm (38,700 g) at 4 °C in a Sorvall SS34 rotor. SDS-PAGE revealed that the anti-PD-1 scFv was in the pellet (Fig. 2A; lane 4). Therefore, a urea/high pH-based protocol [37] was used to extract the anti-PD-1 scFv. In brief, the pellet was re-suspended in 100 ml of Buffer B (100 mM Tris.HCl pH 12.5, 2 M urea, 20 mM imidazole, 10% glycerol and 0.02% Tween 80) and incubated at room temperature for 30 min with gentle rocking on a "nutator". Following incubation, the pH was lowered to pH 8.0 via addition of 1 N HCl, while stirring. The suspension was then centrifuged for 20 min at 18,000 rpm at 4 °C in a Sorvall SS34 rotor.

3. Refolding and Ni-NTA Column Chromatography: The solubilized anti-PD1 scFv was mixed with QIAGEN Ni-NTA agarose beads (~2 ml of beads) for 1 h at 4 °C with gentle rocking. The Ni-NTA beads, bound to the unfolded anti-PD1 scFv, were then pelleted in a Beckman GS-6R centrifuge at 280 RPM for 10 min; non-bound material was removed by aspiration. As an initial wash, the Ni-NTA agarose resin was re-suspended in Buffer B (5X column volume), incubated for 5 min and then re-pelleted in the GS-6R centrifuge. To refold the anti-PD-1 scFv, the Ni-NTA beads were re-suspended in 10X the bead volume of Buffer C (20 mM Tris.HCl pH 8.0, 100 mM NaCl, 0.1% Triton X-100, 4 mM oxidized glutathione and 4 mM reduced glutathione) and incubated for 30 min at 4 °C. Upon centrifugation at 280 RPM for 10 min, and aspiration of Buffer C, the pellet was re-suspended in 10X column volumes of Buffer D (20 mM Tris.HCl pH 8.0, 100 mM NaCl, 5 mM β-cyclodextrin, 4 mM oxidized glutathione and 4 mM reduced glutathione) and incubated for 1 h at 4 °C. After an additional cycle of centrifugation and aspiration, the pellet was re-suspended in 10X the bead volume of Buffer E (20 mM Tris.HCl pH 8.0 and 0.5 M NaCl). The beads bound to the scFv were then divided into two 1 ml polypropylene disposable columns (QIAGEN) and the resin allowed to settle by gravity.

Prior to elution, the Ni-NTA agarose resin containing the bound anti-PD-1 scFv was washed in ten column volumes of low imidazole "Wash buffer" (20 mM Tris.HCl pH 8.0, 300 mM NaCl, 10% glycerol, 20 mM

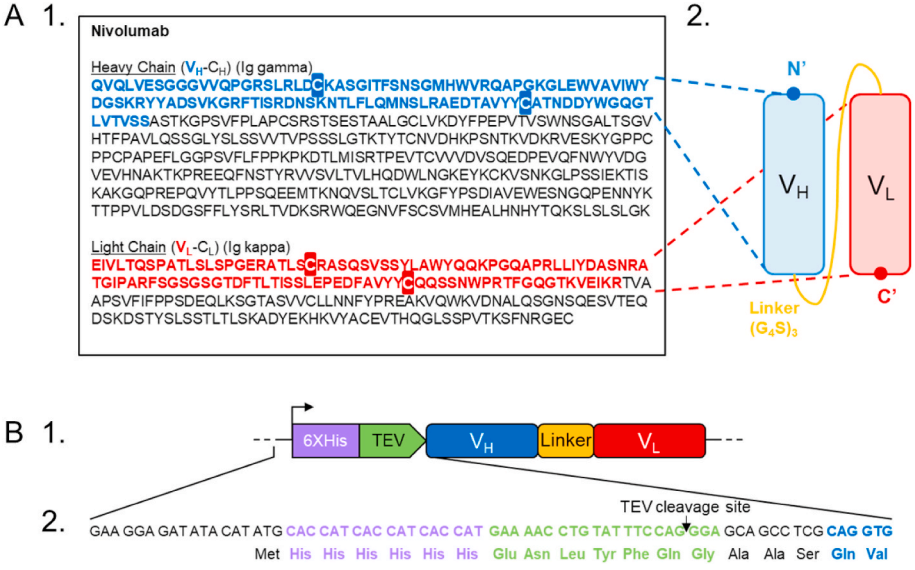

Fig. 1. Sequences used to form the anti-PD-1 scFv. **A1.** The sequences of Nivolumab incorporated into the anti-PD-1 scFv. The V_H sequences used to form the anti-PD-1 scFv are in blue, while the V_L sequences are in red. The two pairs of cysteines used to form the intradomain disulfides (i.e., Cys 23 & 88 in V_L and Cys 22 and 96 in V_H) that are critical for the stability of scFv fragments [97] are highlighted. **A2.** A diagram of the V_L and V_H containing anti-PD-1 scFv; the $(Gly_4S)_3$ linker is symbolized by the yellow line. **B1.** A schematic of the region of plasmid pLIC-His-anti-PD-1 that encodes the anti-PD-1 scFv including the 6X His, TEV cleavage, V_H, $(Gly_4S)_3$ linker and V_L sites. **B2.** An expanded view showing the DNA sequences from the 6X His (in purple) and TEV cleavage sites (in green). The lower line presents the amino acids encoded by these regions, including the Met that establishes the N-terminus of the anti-PD-1 scFv. Finally, presented in blue are the first two amino acids from the V_H domain of Nivolumab (and the corresponding DNA sequence).

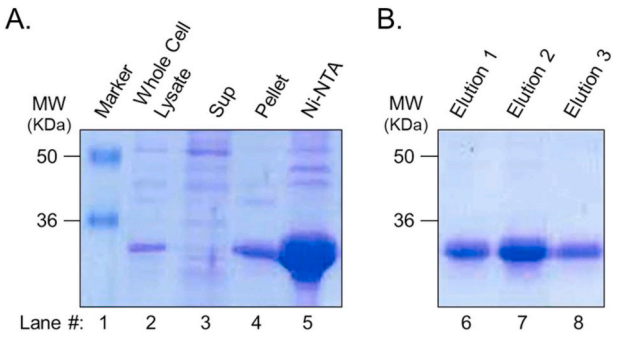

Fig. 2. Protein induction and purification of the anti-PD-1 scFv from *E. coli* BL21 cells. **A.** Representative SDS-PAGE gel showing the distribution of the anti-PD-1 scFv during stages of purification. Pre-stained "SeeBlue Plus 2″ protein size markers (Thermo Fisher) were run in Lane 1. The whole cell lysate following induction with IPTG (20 μl) is shown in Lane 2; a key feature is the prominent band running at the expected location of the anti-PD-1 scFv (~27 kDa). Lane 3, the lysate supernatant (20 μl) following centrifugation at 18,000 RPM. Lane 4, the cell pellet following solubilization in Buffer B (20 μl). Lane 5, an aliquot of the loaded Ni-NTA resin (~5 μl) after *in situ* renaturation of the anti-PD-1 scFv and washing with ten column volumes of low imidazole "wash buffer". **B.** To elute the anti-PD-1 scFv from the Ni-NTA column, 10 mls of "elution buffer" was applied and 1 ml fractions were collected. The peak fractions of the anti-PD-1 scFv were identified by spotting aliquots onto Whatman filter paper and staining with Coomassie Brilliant Blue, as well as subsequent analyses of 20 μl aliquots by SDS-Page (lanes 6–8). Finally, our yield of purified anti-PD-1 scFv was lower than expected (i.e., ~1 mg from 2.5 g of bacterial cell pellet). It is noted that during elution with 300 mM imidazole not all of the anti-PD-1 scFv was removed from the Ni-NTA column. In addition, not all of the scFv was recovered from the pellet during the urea/high pH-based extraction (data not shown). While we have yet to determine why these purification steps are sub-optimal, a likely contributor is insoluble aggregation of some fraction of the scFv.

imidazole and 0.02% Tween 80). The bound anti-PD-1 scFv was then eluted with 5 ml of "Elution buffer" (20 mM Tris.HCl pH 8.0, 0.3 M NaCl, 10% glycerol, 0.02% Tween 80 and 300 mM imidazole) and ten 0.5 ml fractions were collected. To immediately lower the pH away from the pI of the scFv (~8.65; determined using the ExPASy WEB site), each Eppendorf collection tube contained 0.5 ml of 2X collection buffer (25 mM Hepes, pH 6.8, 0.4 M NaCl, 100 mM Na citrate dihydrate (pH 6.0), 25% glycerol and 0.02% Tween 80). Following elution, the peak fractions of the anti-PD-1 scFv were detected by Coomassie Blue staining of aliquots spotted onto Whatman filter paper. Fractions containing the highest concentrations of the anti-PD-1 scFv were then dialyzed overnight at 4 °C against 2 L of "Storage buffer" (25 mM HEPES, pH 6.8, 0.125 M NaCl, 0.2 M Mannitol, 21.5 μM EDTA, 0.02% Tween 80, 40 mM Na citrate dihydrate and 20% glycerol). The purified anti-PD-1 scFv (~0.2 mg/ml) was stored at −80 °C until needed. Regarding the determination of the concentration of the purified anti-PD-1 scFv; using the ExPASy portal, the extinction coefficient for the 6X His containing anti-PD-1 scFv at 280 nm was determined to be 51,130 M^{-1} cm^{-1}. After obtaining the spectra of the purified anti-PD-1 on an Agilent 8453 UV–visible spectrophotometer, and subtracting the spectra of the Storage buffer, the concentration of anti-PD-1 scFv samples was determined using Beer's Law. The accuracy of this approach was confirmed by SDS-PAGE of aliquots of the purified anti-PD-1 scFv and subsequent quantitation using ImageJ.

2.2. Modeling the structure of the anti-PD-1 scFv

The program SWISS-MODEL [38] was used to predict the structure of the 27.1 kDa anti-PD-1 scFv; this structure was then displayed in PyMol [39]. To superimpose the predicted structure of the anti-PD-1 scFv with the corresponding region of Nivolumab, the coordinates for the co-structure of human PD-1 bound to the Fab region of Nivolumab [40] were obtained from the PDB (5WT9). The internal alignment function of PyMol was then used to align the predicted structure of the anti-PD-1 scFv with the corresponding region of Nivolumab (calculation of alignment was placed with a restriction to alpha carbons of the backbone of the proteins).

2.3. A molecular model demonstrating that the anti-PD-1 scFv bound to PD-1 will block binding to PD-L1

The residues on PD-1 that bind to the Fab region of nivolumab [40, 41] and those that bind to PD-L1 [42], were previously reported. The anti-PD-1 scFv was positioned opposite the nivolumab-binding site via standard procedures. In brief, starting with the nivolumab/PD-1 co-structure [40], the predicted structure of the anti-PD-1 scFv (described herein) was aligned to nivolumab using the alignment function of PyMol [43].

2.4. Western blotting

Human PD-1 was purchased from ACROBiosystems and the indicated amounts were separated by SDS-PAGE on a 10% acrylamide gel. The PD-1 protein, and BSA control, was then transferred to a PVDF membrane (Millipore). After overnight blocking at 4 °C with 5% dry milk in TBST (20 mM Tris (pH 7.5), 137 mM NaCl and 0.1% Tween-20) the membrane was incubated for 1 h at RT with the purified anti-PD-1 scFv (0.25 μg/ml) in ~20 ml of TBST containing 2% dry milk. The 6xHis tag on the scFv was subsequently detected using a horseradish peroxidase-conjugated anti-polyhistidine monoclonal antibody ((Abcam: ab49781 diluted 1:2500) and the blot was developed using an enhanced chemiluminescence detection kit (Millipore).

2.5. Determining the IC_{50} of the anti-PD-1 scFv for PD-1

BPS Bioscience has developed a FRET-based high-throughput assay that measures the effectiveness of molecules at inhibiting the PD-1/PD-L1 interaction http://bpsbioscience.com/pd-1-pd-l1-tr-fret-72038. In brief, to identify a PD-1/PD-L1 binding inhibitor, a 384-well time-resolved fluorescence resonance energy transfer (TR-FRET)-based assay was used that measures the binding of biotinylated PD-L1 (PD-L1-biotin) to europium-labeled PD-1 (PD-1-Eu). To conduct the assay, PD-L1-biotin, PD-1-Eu and streptavidin-allophycocyanin (SA-APC) are incubated in the presence of a range of compound concentrations. In the absence of inhibition, the complex PD-L1-biotin/SA-APC is bound to PD-1-Eu and allows the resonance energy transfer from the donor Eu to the acceptor APC; as a result, the final fluorescence emission is high. In the presence of an inhibitor, the interaction between PD-L1-biotin/SA-APC and PD-1-Eu is blocked; therefore, the energy transfer is disrupted and fluorescence emission from the acceptor is low.

3. Results

3.1. The isolation of an anti-PD-1 scFv from E. coli

The residues from the V_H and V_L chains of Nivolumab used to form the ~27 kDa anti-PD-1 scFv are presented in Fig. 1A1 (blue and red sequences, respectively). The regions comprising the V_H and V_L chains were connected via the $(Gly_4S)_3$ linker [35] that is depicted in Fig. 1A2 (yellow line; C-terminus of V_H linked to the N-terminus of V_L). The sequences encoding the anti-PD-1 scFv were purchased as a gBlock from IDT and cloned into plasmid pLIC (Materials and Methods). A schematic of the region of plasmid pLIC-His-anti-PD-1, that encodes the V_H and V_L regions of the anti-PD-1 scFv, as well as the N-terminal 6xHis and TEV protease sites, is presented in Fig. 1B1. Furthermore, the DNA sequences of the 6xHis and TEV protease regions of the vector are presented in Fig. 1B2. Immediately below the DNA sequence are the amino acids encoded by these residues, including the Met used to initiate the 6xHis

and TEV protease site-containing anti-PD-1 scFv.

The procedure used to express the anti-PD-1 scFv in *E. coli* BL21, and the Ni-NTA resin-based protocol used to purify the molecule, are also described in the Materials and Methods section. It is stressed that the purified anti-PD-1 scFv contains the N-terminal 6xHis tag and the TEV protease cleavage site. SDS-PAGE analysis of aliquots taken during key stages of purification are presented in Fig. 2A (lanes 2–5). Additional SDS-PAGE analyses (Fig. 2B; lanes 6–8) established that the isolation procedure resulted in the purification to apparent homogeneity of the anti-PD-1 scFv. Finally, using this approach, approximately 1 mg of the anti-PD-1 scFv was purified from 4 g of bacterial cell pellet.

3.2. The predicted structure of the anti-PD-1 scFv

A. Phyre 2 based model of the scFv: A model of the structure of the anti-PD-1 scFv was obtained using the program Phyre 2 [43]. A ribbon diagram of the predicted structure of the scFv that includes the V_H (blue), V_L (red) and $(Gly_4S)_3$ linker (yellow) regions of the molecule, is presented in Fig. 3A. The side chains for the C-terminal arginine (Fig. 1A1) are shown as red spheres. Residues of the molecule including the N-terminal 6xHis [44] and TEV protease site (Fig. 1B1) are, however, likely to be unstructured (see legend) and therefore, these residues were not included in the modeling studies. Thus, the structure presented in Fig. 3A depicts only the predicted location of the N-terminus of the V_H chain. Finally, to help locate the region of the anti-PD-1 scFv involved in binding to PD-1 [40,41], Fig. 3A also depicts where PD-1, symbolized by the dotted circle, would dock to the surface of anti-PD-1 scFv.

B. Superposition of the scFv model onto the structure of full-length nivolumab: The co-structure of the nivolumab-Fab complex bound to human PD-1 has been reported [41,45]. Therefore, as an initial test of the validity of the predicted structure of the anti-PD-1 scFv, the program Coot [46] was used to superimpose the model of the anti-PD1 scFv (Fig. 3A) onto the co-structure of nivolumab-Fab bound to PD-1 (Fig. 3B; the nivolumab-Fab/PD-1 co-structure is shown in gray). These analyses establish that there is extensive alignment between the two structures (the RMSD for the superimposed structures was 1.049), suggesting that the predicted structure is a reasonable working model of the anti-PD1 scFv.

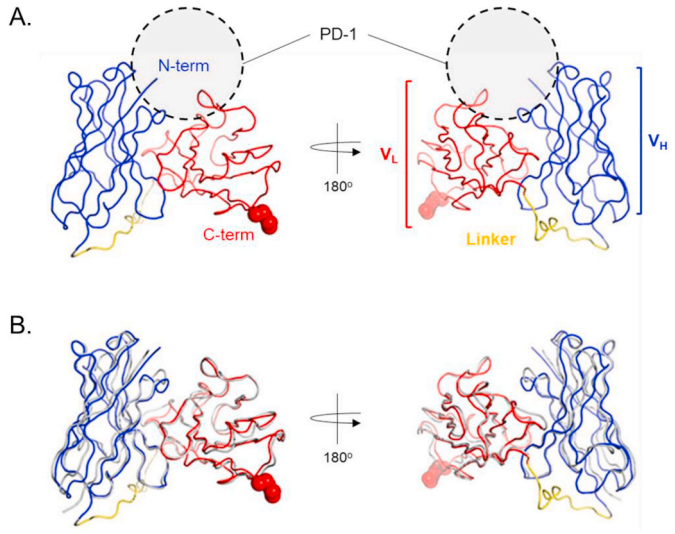

Fig. 3. Models depicting the predicted structural features of the anti-PD-1 scFv. **A**. A model of the anti-PD1 scFv antibody generated using the program Phyre 2 [43]. The V_H domain is shown in blue, the C-terminal V_L region is shown in red and the $(Gly_4S)_3$ linker is shown in yellow. The location of the side chain of the C-terminal (abbreviated C-term) arginine is indicated. Regarding sequences in the N-terminal region, TEV protease recognizes a linear epitope and His tags are known to be unstructured; therefore, the 6X His and TEV cleavage sites are not included in this model. As a result, the depicted N-terminal (abbreviated N-term) is only an approximation. Finally, the circular dotted line symbolizes PD-1 and is used to establish the relative location of the surface on the anti-PD-1 scFv that binds to PD-1 (based on the nivolumab-Fab complex bound to human PD-1 [41]). **B**. Superimposition of the predicted structure of the anti-PD-1 scFv (blue, red and yellow ribbons) onto the corresponding region of the nivolumab-Fab co-structure [41]; shown in gray) that was bound to human PD-1.

3.3. The purified anti-PD-1 scFv selectively binds to human PD-1 and blocks interactions with PD-L1

A. The antigen-binding site on the anti-PD-1 scFv: Fig. 4A presents a space-filling model of the anti-PD-1 scFv that depicts both the predicted antigen-binding region (shown in cyan) and residues in nivolumab (shown in teal) that are known to interact with PD-1 [40,41]. Importantly, residues derived from the $(Gly_4S)_3$ linker are not predicted to be in a position to obscure the residues used to bind to PD-1. However, given the previously discussed uncertainties regarding the location(s) of the N-terminal 6xHis and TEV protease regions, these N-terminal sequences might be situated on the surface of the anti-PD-1 scFv in a manner that could interfere with binding to PD-1. Therefore, to eliminate this possibility, and to confirm the hypothesis that we had identified the amino acid residues needed for a functional anti-PD-1 scFv, we tested if the 6xHis and TEV protease site-containing anti-PD-1 scFv binds to purified PD-1.

B. The anti-PD-1 scFv binds to human PD-1: To determine if the purified anti-PD-1 scFv binds to PD-1, full-length human (h) PD1 was purchased from ACROBiosystems and subjected to SDS-PAGE. A Western blot was then performed, using the 6xHis anti-PD-1 scFv as the primary antibody and an anti-polyhistidine monoclonal Ab conjugated to HRP as the secondary Ab (materials and methods). Inspection of Fig. 4B establishes that the anti-PD-1 scFv bound to either 50 or 100 ng of purified hPD1, but not to 100 ng of BSA (compare lane 1 with lanes 3–4). Therefore, it was concluded that the anti-PD-1 scFv is active and that the N-terminal 6xHis and TEV protease regions do not obscure residues needed for binding to PD-1. Finally, it is noted that the full-length human PD1 from ACROBiosystems is heavily glycosylated; therefore, this molecule does not run as a distinct species.

C. Determining the half maximal inhibitory concentration of the anti-PD-1 scFv needed to disrupt the PD-1/PD-L1 interaction: The IC_{50} of molecules that bind to purified PD-1 can be determined using a FRET-

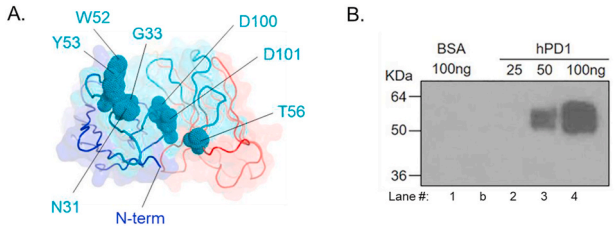

Fig. 4. A surface representation of the anti-PD-1 scFv showing residues needed for binding to PD-1 and evidence that the anti-PD-1 scFv binds to PD-1. **A.** A view of the anti-PD-1 scFv showing the locations of residues (in teal) needed for binding to PD-1 (determined using the nivolumab-Fab/PD-1 co-structure [41]). Based on this model, it was predicted that the PD-1 binding surface on the anti-PD-1 scFv is not blocked by the $(G_4S)_3$ linker. However, since the location (s) of the 6X His and TEV cleavage sequences are unknown, the modeling studies could not address whether residues from the N-terminus of the anti-PD-1 scFv obscure the residues needed for PD-1 binding. **B.** Western blot-based evidence that the anti-PD-1 scFv binds to human PD-1. The Western blot was conducted with the indicated amounts (25–100 ng) of human PD-1 (lanes 3–5). In contrast, binding was not detected to 100 ng of the control BSA sample (lane 2). The secondary Ab was an anti-polyhistidine monoclonal Ab conjugated to HRP (Abcam: ab49781). Protein size markers were also loaded on the gel; the relative mobilities of the individual markers are indicated. Finally, "b" stands for blank.

based competition assay developed by BPS Bioscience. A depiction of this FRET assay is presented in Fig. 5A and the individual symbols are defined in the figure legend. It is stressed that this assay measures the extent to which a molecule that binds to PD-1 is able to disrupt the PD-1/PD-L1 interaction. Using this assay, it was established that the anti-PD-1 scFv disrupted the PD-1/PD-L1 interaction with an IC50 of 26 nM (Fig. 5B1). Additional evidence for tight binding is the observation that the anti-PD-1 scFv maintained ~15% inhibition at 6 nM. As a control, a second reaction was conducted with the nonpeptidic PD-1/PD-L1 complex inhibitor BMS 202 (Fig. 5B2). In this assay, the IC50 for BMS202 was determined to be 8.2 nM, which compares favorably to the previously published value of 18 nM [47]. In summary, the anti-PD-1 scFv binds tightly to human PD-1 and this association blocks the further interaction between PD-1 and PD-L1.

3.4. Evidence that the disruption of the PD-1/PD-L1 interaction by the anti-PD-1 scFv is due to steric exclusion

Nivolumab is known to block the PD-1/PD-L1 interaction owing to a steric clash resulting from residues in the V_L region of nivolumab obscuring the PD-L1 binding site ([41]; reviewed in Refs. [48,49]). As a test of the hypothesis that the V_L region present in the anti-PD-1 scFv blocks PD-L1 binding in a similar manner, we modeled the docking of the anti-PD-1 scFv to PD-1 and then analyzed whether the residues needed for binding by PD-L1 are obscured.

In Fig. 6 (left panel), the residues on the surface of PD-1 that comprise the binding site for PD-L1 [42] are shown in orange, while those used to bind nivolumab are colored in green. Inspection of Fig. 6 (right panel) reveals that upon binding of the anti-PD-1 scFv (depicted as the blue, yellow and red ribbon diagram) to PD-1 that the PD-L1 binding site is blocked. Thus, our modeling studies indicate that the same mechanism is used by the anti-PD-1 scFv, and full-length nivolumab, to block the PD-1/PD-L1 interaction.

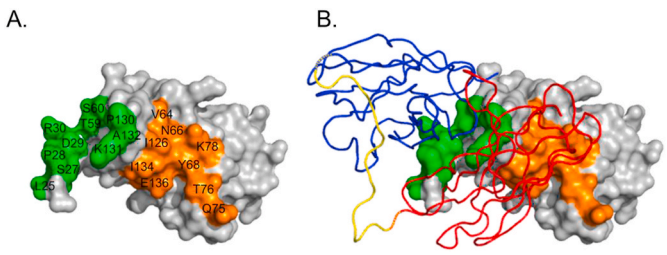

Fig. 6. A model of the surface of PD-1 illustrating that the binding site for PD-L1 would be obscured upon binding of the anti-PD-1 scFv to PD-1. **A.** Depiction of the surface of PD-1 showing residues utilized for binding to Nivolumab ([40]; shown in green) and those required for binding to PD-L1 ([42]; shown in orange). **B.** Upon docking of the anti-PD-1 scFv to PD-1, using the residues needed to bind Nivolumab, it is apparent that the V_L region of the anti-PD-1 scFv (in red) would obscure the PD-1 residues needed for binding to PD-L1.

4. Discussion

Full-length anti-PD1 monoclonal Abs have been used with remarkable success to treat certain cancers (reviewed in Refs. [4,48,50–53]). However, there are limitations associated with full-length Ab based immune checkpoint therapies (reviewed in Ref. [54]). For instance, the majority of patients will not respond, or will respond only incompletely, to PD-1 or PD-L1 inhibitors (reviewed in Refs. [3,4,7,16]). Furthermore, intact immunoglobulins are too large for effective tumor penetration and their slow clearance from the blood can result in high retention in multiple organs, including the liver [55]. Therefore, there is a need to pursue the development of additional reagents for immune checkpoint therapies, such as the anti-PD-1 scFv described herein.

That scFvs can be used as therapeutic agents in checkpoint and cancer therapy has been previously established (reviewed in Ref. [56]). For instance, an scFv derivative of the PD-L1 targeting antibody Avelumab has been reported [57], as has an scFv targeting human CTLA-4 [58]. Furthermore, Rafiq et al. reported that CAR-T cells that secrete a PD-1-blocking scFv enhanced the survival of mice harboring several

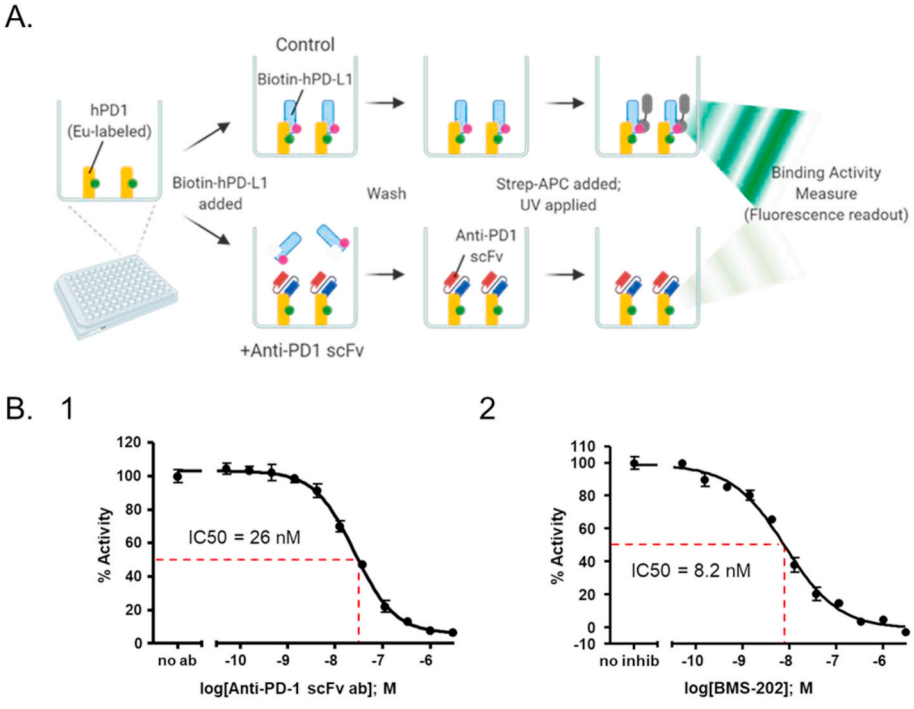

Fig. 5. Determining the IC50 for the anti-PD1 scFv. **A.** An overview of the BPS Bioscience competition assay, which was used to determine the concentration of the anti-PD-1 scFv needed for 50% inhibition of binding of PD-L1 to human PD-1. The anti-PD-1 scFv is symbolized by the linked red and dark blue rectangles, human PD-1 by the yellow rectangle and PD-L1 by the light blue images. Note that in this assay, PD-1 is linked to europium (Eu (green dot); PD-1-Eu), human PD-L1 is conjugated to biotin (purple dot) and the reaction takes place in the presence of streptavidin-allophycocyanin ((SA-APC); gray structure bound to biotin). In the absence of inhibitor, PD-L1 biotin forms a complex with SA-APC and PD-1-Eu. Upon excitation by U.V. light, there is an energy transfer from the donor Eu to the SA-APC acceptor and thus high fluorescence emission (top row). In the presence of an inhibitor that binds to PD-1 (e.g., the anti-PD-1 scFv), the interaction between PD-L1-biotin/SA-APC and PD-1-Eu is blocked. Therefore, the U.V. dependent energy transfer is disrupted and fluorescence emission from the acceptor is low (bottom row). **B.** Use of the BPS Bioscience competition assay to determine the IC50 of the anti-PD-1 scFv for human PD-1. The IC50 of the anti-PD-1 scFv, derived from the three separate experiments shown in the plot, was determined to be 26 nM (Fig. 5B1). As a control, the competition assay was repeated in the presence of the small molecule BMS-202; based on three separate assays, the IC50 was determined to be 8.2 nM (Fig. 5B2).

different types of tumors [59]. They also reported that the scFvs secreted by CAR-T cells remain locally in the tumor microenvironment. In addition, a novel method was used to generate libraries of scFvs targeting PD-1, that were subsequently re-engineered into full-length monoclonal Abs for additional validation [60].

The clinical significance of targeting the PD-1/PD-L1 axis by full-length Abs, or Ab fragments, is further illustrated by the fact that a broad range of antiviral immune responses is regulated by the PD-1/PD-L1 interaction. For instance, exhausted CD8 T cells present in mice chronically infected with lymphocytic choriomeningitis virus (LCMV) had up-regulated PD-1 levels and antibodies that blocked the PD-1/PD-L1 interaction restored T-cell responses [61]. Furthermore, a wide range of viruses, including Hepatitis B and C [62] and HIV [63], are known to up-regulate PD-1 ligands on both hematopoietic and non-hematopoietic cells (reviewed in Ref. [64,65]). The possibility of treating SARS-CoV-2 with immune checkpoint inhibitors has also been discussed [66]. Of additional interest, treatment with anti-PD-1 antibodies led to durable tumor regression in patients with Merkel Cell Carcinoma (e.g. Refs. [67–70]) and positive responses in PML patients (reviewed in Ref. [65,71]). In view of these reports, the anti-PD-1 scFv, or second-generation derivatives, may have additional efficacy as both anti-viral agents and reagents to combat virally induced diseases.

In terms of the mechanism utilized by the anti-PD-1 scFv to disrupt the PD-1/PD-L1 interaction, the purified anti-PD-1 scFv has an IC50 of 26 nM, while the IC50 of full-length nivolumab is 2.52 nM (as determined by surface plasmon resonance [72]). Thus, the IC50s, obtained using two separate methods, are not identical. Whether this difference is because the anti-PD-1 scFv is actually 10-fold weaker than full-length nivolumab, or if only 10% of the scFv molecules are active, remains to be determined. Nevertheless, the tight binding of the anti-PD-1 scFv to PD-1 is in keeping with previous experiments that demonstrated that scFv fragments that contain the complete antigen-binding site of an antibody, and have not undergone reorientation of the two domains, have the same monomeric binding affinity as the parental monoclonal antibody [73]. Furthermore, based on the design of the BPS Bioscience FRET-based assay, it is apparent that once tightly bound to PD-1, the anti-PD-1 scFv blocks the ability of PD-L1 to interact with PD-1. Indeed, our modeling studies indicate that the anti-PD-1 scFv blocks the PD-1/PD-L1 interaction via the same steric exclusion mechanism utilized by full-length Nivolumab (reviewed in Ref. [48]).

Regarding possible clinical advantages of the purified anti-PD-1 scFv, high tumor penetrance is an established clinical advantage of relatively small scFv fragments [31]. An additional property of the scFvs is that owing to their high dissociation rates, they are cleared relatively rapidly from the body [55,74]. This has been suggested to be an advantage [6], since agents that clear rapidly from the circulation, relative to intact IgGs, have the potential for lower toxicities. However, if rapid clearance is demonstrated to be a limitation of the anti-PD-1 scFv, the half-life and stability of the anti-PD-1 scFv could be increased by various modifications, including linkage to polyethylene glycol ([75]; reviewed in Ref. [30]). Alternatively, its size could be increased to ~60 kDa using techniques such as peptide linker dimerization [74,76]. Dimerization would be expected to increase the avidity of the anti-PD-1 scFv for PD-1 (e.g. Refs. [30,77]), while its increased size would likely reduce clearance by the kidney [74].

A related consideration is that owing to Fc dependent interactions with a range of cellular receptors [78], many full-length Abs have the potential to induce cellular effector functions (including targeted cell lysis and phagocytosis (e.g. Ref. [79,80]). However, the IgG4 Ab subclass is an exception. They have a low affinity for Fc and C1q receptors; thus, they poorly activate host effector functions [81]. Indeed, the IgG4 isotype is the preferred class for immunotherapy when host effector function(s) are undesirable [81]. As a result, the anti-tumor effectiveness of nivolumab, an IgG4 monoclonal Ab, is not dependent upon the induction of host effector functions. Similarly, since the anti-PD-1 scFv does not contain an Fc region, it is unlikely to induce cellular effector functions. A related advantage of the anti-PD-1 scFv is that full-length anti-PD-1 mAbs are captured within minutes from the surface of T-cells by tumor-associated macrophages and the Fc domains of the mAbs play a critical role in this interaction [82]. Since the anti-PD-1 scFv does not contain an Fc domain, its binding to T-cells should be less prone to disruption by tumor-associated macrophages.

An additional concern is that checkpoint therapies utilizing full-length antibodies are associated with "immune-related adverse effects" (IRAEs; ([83,84]; reviewed in Ref. [85]). For instance, IRAEs occur in up to 70% of patients treated with PD-1/PD-L1 antibodies (reviewed in Ref. [85]) and serious (i.e., grade 3 or 4) adverse events were associated with many patients being treated with nivolumab ([49,51,86,87]; reviewed in Ref. [50]). In addition, the frequency of adverse events was much higher when full-length nivolumab was used in combination therapy with CTLA-4 targeting ipilimumab [88]. Addressing IRAE related concerns, it was proposed that CAR-T based localized delivery of the much smaller anti-PD-1 scFvs to tumors may decrease the IRAEs associated with checkpoint blockades [59]. Likewise, scFvs, including the anti-PD-1 scFv described herein, may reduce IRAEs owing to related properties, such as their inherently lower immunogenicity [33].

Given the results presented herein, and the properties of scFvs summarized above, it is apparent that continued characterization and modification of the anti-PD-1 scFv is warranted. As noted previously, the anti-PD-1 scFv could serve as the building block for the production of larger derivatives, including bi-specific and multi-variant antibody fragments (e.g., Refs. [89–92]; reviewed in Ref. [93]). Moreover, to enhance diagnostic tests for the presence of PD-1 in tumor biopsies, the anti-PD-1 scFv could be coupled to fluorescent protein domains. The anti-PD-1 scFv could also be coupled to radioactive tracers and used in whole-body imaging studies (e.g. Ref. [94]). Regarding the fact that the anti-PD-1 scFv is purified from *E. coli*, since the 1980's there have been a number of recombinant biopharmaceuticals produced in *E. coli* (reviewed [95]) and biopharmaceuticals produced in *E. coli* include antibodies (e.g. Ref. [96]). Finally, the high cost of production of therapeutic antibodies in mammalian cell culture can limit their availability to patients (e.g. Ref. [80]); therefore, a significant incentive for further studies of the anti-PD-1 scFv purified from *E. coli* is that it can be manufactured at greatly reduced costs.

CRediT authorship contribution statement

Jong Shin: Investigation, Software, Data curation, Methodology. **Paul J. Phelan:** Investigation, Software, Methodology, Writing - review & editing. **Ole Gjoerup:** Conceptualization, Methodology. **William Bachovchin:** Conceptualization. **Peter A. Bullock:** Conceptualization, Methodology, Supervision, Writing - review & editing.

Acknowledgments

We thank David Sanford, Gretchen Meinke and Geoffrey Sunshine for helpful discussions and Andrew Bohm for advice on using the Avestin. This work was supported by funding from RepVir.

References

[1] P. Sharma, J.P. Allison, The future of immune checkpoint therapy, Science 348 (2015) 56–61.
[2] P.C. Tumeh, et al., PD-1 blockade induces responses by inhibiting adaptive immune resistance, Nature 515 (2014) 568–571.
[3] S.L. Topalian, C.G. Drake, D.M. Pardoll, Immune checkpoint blockage: a common denominator approach to cancer therapy, Canc. Cell 27 (2015) 450–461.
[4] D.B. Page, M.A. Postow, M.K. Callahan, J.P. Allison, J.D. Wolchok, Immune modulation in cancer with antibodies, Annu. Rev. Med. 65 (2014) 185–202.
[5] D.M. Pardoll, The blockade of immune checkpoints in cancer immunotherapy, Nat. Rev. Canc. 12 (2012) 252–264.
[6] I. Mellman, G. Coukos, G. Dranoff, Cancer immunotherapy comes of age, Nature 480 (2011) 480–489.

[7] D.S. Chen, I. Mellman, Elements of cancer immunity and the cancer-immune set point, Nature 541 (2017) 321–330.
[8] H. Dong, S.E. Strome, D.R. Salomao, et al., Tumor-associated B7-H1 promotes T-cell apoptosis: a potential mechanism of immune evasion, Nat. Med. 8 (2002) 1039–1044.
[9] M. Ahmadzadeh, L.A. Johnson, B. Heemskerk, J.R. Wunderlich, M.E. Dudley, D. E. White, S.A. Rosenberg, Tumor antigen-specific CD8 T cells infiltrating the tumor express high levels of PD-1 and are functionally impaired, Blood 114 (2009) 1537–1544.
[10] K.S. Sfanos, T.C. Bruno, A.K. Meeker, A.M. DeMarzo, W.B. Isaccs, C.G. Drake, Human prostate-infiltrating CD8+ T lymphocytes are oligoclonal and PD-1 +, Prostate 69 (2009) 1694–1703.
[11] G.J. Freeman, A.J. Long, Y. Iwai, K. Bourque, T. Chernova, H. Nishimura, L.J. Fitz, N. Malenkovich, T. Okazaki, M.C. Byrne, et al., Engagement of the PD-1 immunoinhibitory receptor by a novel B7 family member leads to negative regulation of lymphocyte activation, J. Exp. Med. 192 (2000) 1027–1034.
[12] Y. Ishida, Y. Agata, K. Shibahara, T. Honjo, Induced expression of PD-1, a novel member of the immunoglobulin gene superfamily, upon programmed cell death, EMBO J. 11 (1992) 3887–3895.
[13] M.E. Kier, M.J. Butte, G.J. Freeman, A.H. Sharpe, PD-1 and its ligands in tolerance and immunity, Annu. Rev. Immunol. 26 (2008) 677–704.
[14] M.A. Postow, M.K. Callahan, J.D. Wolchok, Immune checkpoint blockade in cancer therapy, J. Clin. Oncol. 33 (2015) 1974–1982.
[15] I. Marquez-Rodas, P. Cerezuela, A. Soria, A. Berrocal, A. Riso, M. Gonzalez-Cao, S. Martin-Algarra, Immune checkpoint inhibitors: therapeutic advances in melanoma, Ann. Transl. Med. 3 (2015) 267.
[16] D.S. Chen, I. Mellman, Oncology meets immunology: the cancer-immunity cycle, Immunity 39 (2013) 1–10.
[17] R.S. Herbst, J.C. Soria, M. Kowanetz, G.D. Fine, O. Hamid, M.S. Gordon, J. A. Sosman, et al., Predictive correlates of response to the anti PD-L1 antibody MPDL3280A in cancer patients, Nature 515 (2014) 563–567.
[18] A.B. Frey, Suppression of T cell responses in the tumor microenvironment, Vaccine 33 (2015) 7393–7400.
[19] L. Chen, Co-inhibitory molecules of the B7-CD28 family in the control of T-cell immunity, Nat. Rev. Immunol. 4 (2004) 336–347.
[20] Y. Iwai, M. Ishida, Y. Tanaka, T. Okazaki, T. Honjo, N. Minato, Involvement of PD-L1 on tumor cells in the escape from host immune cells in the escape from host immune system and tumor immunotherapy by PD-L1 blockage, Proc. Natl. Acad. Sci. U.S.A. 99 (2002) 12293–12297.
[21] J.R. Brahmer, L. Horn, S.J. Antonia, D.R. Spigel, L. Ghandhi, L.V. Sequist, V. Sankar, C.M. Ahlers, J.M. Wigginton, G. Kollia, Survival and long-term follow-up of the phase I trial of nivolumab (Anti-PD-1; BMS-936558; ONO-4538) in patients withe previously treated advanced non-small cell lung cancer (NSCLC), J. Clin. Oncol. 31 (2013) 8030.
[22] C.G. Drake, D.F. McDermott, M. Sznoi, T.K. Choueirie, H.M. Kluger, J.D. Powderly, D.C. Smith, V. Sankar, A.A. Gutierrez, J.M. Wigginton, et al., Survival, safety, and respnse duration results of nivolumab (Anti-PD-1;BMS-936558; ONO-4538) in a phase I trial in patients with previously treated metastatic renal cell carcinoma (mRCC): long-term patient follow-up, J. Clin. Oncol. 31 (2013) 4514.
[23] M. Sznol, H.M. Kluger, F.S. Hodi, D.F. McDermott, R.D. Carvajal, D.P. Lawrence, S. L. Topalian, M.B. Atkins, J.D. Powderly, W.H. Sharfman, et al., Survival and long-term follow-up of safety and response in patients with advanced melanoma (MEL) in a phae I trial of nivolumab (anti-PD-1; BMS-936558; ONO-4538), J. Clin. Oncol. 31 (2013) CRA9006.
[24] S.L. Topalian, M. Sznoi, J.R. Brahmer, D.F. McDermott, D.C. Smith, S.N. Gettinger, J.M. Taube, C.G. Drake, D.M. Pardoll, et al., Nivolumab (anti-PD-1); BMS-936558; ONO-4538) in patients with advanced solid tumors: surviral and long-term safety in a phase I trail, J. Clin. Oncol. 31 (2013) 3002.
[25] J.R. Brahmer, C.G. Drake, I. Wollner, J.D. Powderly, J. Picus, W.H. Sharfman, E. Stankevich, A. Pons, T.M. Salay, T.L. McMiller, et al., Phase I study of single-agent anti-programmed death-1 (MDX-1106) in refractory solid tumors: safety, clinical activity, pharmacodynamics, and immunological correlates, J. Clin. Oncol. 28 (2010) 3167–3175.
[26] O. Hamid, C. Robert, A. Daud, F.S. Hodi, W.J. Hwu, R. Kefford, J.D. Wochok, P. Hersey, R.W. Joseph, J.S. Weber, et al., Safety and tumor reponses with Iambrolizumab (anti-PD-1) in melanoma, N. Engl. J. Med. 369 (2013) 134–144.
[27] R.E. Bird, K.D. Hardman, J.W. Jacobson, S. Johnson, B.M. Kaufman, S.M. Lee, T. Lee, S.H. Pope, G.S. Riorda, M. Whitlow, Single-chain antigen-binding proteins, Science 242 (1988) 423–426.
[28] J.S. Huston, D. Levinson, M. Mudgett-Hunter, M.S. Tai, J. Novotny, M. N. Margolies, R.J. Ridge, R.E. Bruccoleri, E. Haber, R. Crea, H. Oppermann, Protein engineering of antibody binding sites: recovery of specific activity in an anti-digoxin single-chain Fv analogue produced in *Escherichia coli*, Proc. Natl. Acad. Sci. U.S.A. 85 (1988) 5879–5883.
[29] Z.A. Ahmad, S.K. Yeap, A.M. Ali, W.Y. Ho, N.B.M. Alitheen, M. Hamid, scFv antibody: principles and clinical application, Clin. Dev. Immunol. 2012 (2012) 1–15.
[30] P. Holliger, P.J. Hudson, Engineered antibody fragments and the rise of single domains, Nat. Biotechnol. 23 (2005) 1126–1136.
[31] T. Yokota, D.E. Milenic, M. Whitlow, J. Schlom, Rapid tumor penetration of a single-chain Fv and comparison with other immunoglobulin forms, Canc. Res. 52 (1992) 3402.
[32] G.P. Adams, J.E. McCartney, M.S. Tai, H. Oppeermann, J.S. Huston, W.F. Stafford, M.A. Bookman, I. Fand, L.L. Houston, L.M. Weiner, Highly specific in vivo tumor targeting by monvalent and divalent forms of 741F8 ANTI-C-erbB-2 single-chain Fv, Canc. Res. 53 (1993) 4026.
[33] D.E. Milenic, T. Yokota, D.R. Filpula, A.J. Finkelman, S.W. Dodd, J.F. Wood, M. Whitlow, P. Snoy, J. Schlom, Construction, binding properties, metabolism, and tumor targeting of a single-chain fv derived from the pancarcinoma monoclonal antibody CC49, Canc. Res. 51 (1991) 6363–6371.
[34] K.D. Miller, J. Weaver-Feldhaus, S.A. Gray, R.W. Siegel, M.J. Feldhaus, Production, purification, and characterization of human scFV antibodies expressed in *Saccharomyces cerevisiae, Pichia pastoris*, and *Escherichia coli*, Protein Expr. Purif. 42 (2005) 255–267.
[35] R. Glockshuber, M. Malia, I. Prfitzinger, A. Pluckthun, A comparison of strategies to stabilize immunoglobulin Fv-fragments, Biochemistry 29 (1990) 1362–1367.
[36] D.G. Gibson, Enzymatic assembly of overlapping DNA fragments, Methods Enzymol. 498 (2011) 349–361.
[37] A.K. Patra, R. Mukhopadhyay, R. Mukhija, A. Krishnan, L.C. Garg, A.K. Panda, Optimization of inclusion body solubilization and renaturation of recombinant human growh hormone from *E.coli*, Protein Expr. Purif. 18 (2000) 182–192.
[38] A. Waterhouse, M. Bertoni, S. Bienert, G. Studer, G. Tauriello, R. Gumienny, F. T. Heer, T.A.P. de Beer, C. Rempfer, L. Bordoli, R. Lepore, T. Schwede, SWISS-MODEL: homology modelling of protein structures and complexes, Nucleic Acids Res. 46 (2018) W296–W303.
[39] W.L. DeLano, The PyMOL Molecular Graphics System, Delano Scientific, Palo Alto, CA, USA, 2002.
[40] J.Y. Lee, H.T. Lee, W. Shin, J. Chae, J. Choi, S.H. Kim, H. Lim, T. Won Heo, K. Y. Park, Y.J. Lee, S.E. Ryu, J.Y. Son, J.U. Lee, Y.S. Heo, Structural basis of checkpoint blockade by monoclonal antibodies in cancer immunotherapy, Nat. Commun. 7 (2016) 13354.
[41] S. Tan, H. Zhang, Y. Chai, H.-R. Song, Z. Tong, Q. Wang, J. Qi, G. Wong, X. Zhu, W. J. Liu, S. Gao, Z. Wang, Y. Shi, F. Yang, G.F. Gao, J. Yan, An unexpected N-terminal loop in PD-1 dominates binding by nivolumab, Nat. Commun. 8 (2017) 14369.
[42] K.M. Zak, R. Kitel, S. Przetocka, et al., Structure of the complex of human programmed death 1, PD-1, and its ligand PD-L1, Structure 23 (2015) 2341–2348.
[43] L.A. Kelley, M.J.E. Sternberg, Protein structure prediction on the web: a case study using the Phyre server, Nat. Protoc. 4 (2009) 363–371.
[44] M. Carson, D.H. Johnson, H. McDonald, C. Brouillette, L.J. Delucas, His-tag impact on structure, Acta Crystallogr D Biol Crystallogr 63 (2007) 295–301.
[45] J.Y. Lee, H.T. Lee, W. Shin, J. Chae, J. Choi, S.H. Kim, H. Lim, T.W. Heo, K.Y. Park, Y.J. Lee, S.E. Ryu, J.Y. Son, J.U. Lee, Y.S. Heo, Structural basis of checkpoint blockade by monoclonal antibodies in cancer immunotherapy, Nat. Commun. 7 (2016) 13354.
[46] P. Emsley, B. Lohkamp, W.G. Scott, K. Cowtan, Features and development of Coot, Acta Crystallogr D Biol Crystallogr 66 (2010) 486–501.
[47] K.M. Zak, et al., Structural basis for small molecule targeting of the Programmed death ligand 1 (PD-L1), Oncotarget 7 (2016) 30323–30335.
[48] P. Fessas, H. Lee, S. Ikemizu, T. janowitz, A molecular and preclinical comparison of the PD-1-targeted T-cell checkpoint inhibitors nivolumab and pembrolizumab, Semin. Oncol. 44 (2017) 136–140.
[49] A. Mullard, New checkpoint inhibitors ride the immunotherapy tsunami, Nat. Rev. Drug Discov. 12 (2013) 489–492.
[50] Y. Dong, Q. Sun, X. Zhang, PD-1 and its ligands are important immune checkpoints in cancer, Oncotarget 8 (2017) 2171–2186.
[51] M.A. Postow, J. Chesney, A.C. Pavlick, C. Robert, K. Grossmann, D. McDermott, G. P. Linette, et al., Nivolumab and ipilimumab versus ipilimumab in untreated melanoma, N. Engl. J. Med. 372 (2015) 2006–2017.
[52] L. Guo, H. Zhang, B. Chen, Nivolumab as programmed death-1 (PD-1) inhibitor for targeted immunotherapy in tumor, J. Canc. 8 (2017) 410–416.
[53] J. Larkin, V. Chiarion-Sileni, J.J. Gonzalez, J.J. Grob, C.L. Cowey, C.D. Lao, D. Schadendorf, Combined nivolumab and ipilimumab or monotherapy in untreated melanoma, N. Engl. J. Med. 373 (2015) 23–34.
[54] P.S. Hegde, D.S. Chen, Top 10 challenges in cancer immunotherapy, Cell 52 (2020) 17–35.
[55] D. Colcher, G. Pavlinkova, G. Beresford, B.J.M. Booth, A. Choudhury, S.K. Batra, Pharmacokinetics and biodistribution of genetically-engineered antibodies, Q. J. Nucl. Med. 42 (1998) 225–241.
[56] P.J. Hudson, Recombinant antibody constructs in cancer therapy, Curr. Opin. Immunol. 11 (1999) 548–557.
[57] K. Liu, S. Tan, Y. Chai, D. Chen, H. Song, C. Wei-Hong Zhang, Y. Shi, J. Liu, W. Tan, J. Lyu, S. Gao, J. Yan, J. Qi, G.F. Gao, Structural basis of anti-PD-L1 monoclonal antibody avelumab for tumor therapy, Cell Res. 27 (2017) 151–153.
[58] F. Hosseinzadeh, S. Mohammadi, F. Nejatollahi, Production and evaluation of specific single-chain antibodies against CTLA-4 for cancer-targeted therapy, Reports of Biochemistry and Molecular Biology 6 (2017) 8–14.
[59] S. Rafiq, O.O. Yeku, H.J. Jackson, T.J. Purdon, D.G. van Leeuwen, D.J. Drakes, M. Song, M.M. Miele, Z. Li, P. Wang, S. Yan, J. Xiang, X. Ma, V.E. Seshan, R. C. Hendrickson, C. Liu, R.J. Brentjens, Targeted delivery of a PD-1-blocking scFv by CAR-T cells enhances anti-tumor efficacy *in vivo*, Nat. Biotechnol. 36 (2018) 847–856.
[60] A.S. Adler, R.A. Mizrahi, M.J. Spindler, M.S. Adams, M.A. Asensio, R.C. Edgar, J. Leong, R. Leong, D.S. Johnson, Rare, high-affinity mouse anti-PD-1 antibodies that function in checkpoint blockade, discovered using microfluidics and molecular genomics, mAbs 9 (2017) 1270–1281.
[61] D.L. Barber, E.J. Wherry, D. Masopust, B. Zhu, J.P. Alison, A.H. Sharpe, G. J. Freeman, R. Ahmed, Restoring function in exhausted CD8 T cells during chronic viral infection, Nature 439 (2006) 682–687.
[62] T. Watanabe, A. Bertoletti, T.A. Tanoto, PD-1/PD-L1 pathway and T-cell exhaustion in chronic hepatitis virus invfection, J. Viral Hepat. 17 (2010) 453–458.

[63] C.L. Day, D.E. Kaufmann, P. Kiepiela, et al., PD-1 expression on HIV-specific T cells is associated withT-cell exhaustion and disease progression, Nature 443 (2006) 350–354.
[64] G. Schonrich, M.J. Raftery, The PD-1/PD-L1 Axis and virus infecdtions: a delicate balance, Frontiers in Cellular and Infection Microbiology 9 (2019) 10, 3389.
[65] E.S. Beck, I. Cortese, Checkpoint inhibitors for the treatment of JC virus-related progressive multifocal leukoencephalopathy, Current Opinion in Virology 40 (2020) 19–27.
[66] M. Bersanelli, Controversies about COVID-19 and anticancer treatment with immune checkpoint inhibitors, Immunotherapy 10 (2020) 2217.
[67] P.T. Nghiem, et al., PD-1 blockade with pembrolizumab in advanced Merkel cell carcinoma, N. Engl. J. Med. 374 (2016) 2542–2552.
[68] P.T. Nghiem, S. Bhatia, E.J. lipson, W.H. Sharfman, R.R. Kudchadkar, A.S. Brohl, P. A. Friedlander, A. Daud, H.M. Kluger, S.A. Reddy, et al., Durable tumor regression and overall survival in patients with advanced Merkel cell carcinoma receiving pembrolizumab as first-line therapy, J. Clin. Oncol. 37 (2019) 693–702.
[69] F.M. Walocko, B.Y. Scheier, P.W. Harms, L.A. Fecher, C.D. Lao, Metastatic Merkel cell carcinoma response to nivolumab, Journal of ImmunoTherapy of Cancer 4 (2016) 79–83.
[70] H.I. Kaufman, J. Russell, O. Hamid, S. Bhatia, P. Terheyden, S.P. D'Angelo, K. C. Shir, Anelumab in patients with chemotherapy-refractory metastatic Merkel cell carcinoma: a multicentre, single-group, open-label, phase 2 trial, Lancet Oncol. 17 (2016) 1374–1385.
[71] I. Cortese, P. Muranski, Y.E. Enose-Akahata, S.K. Ha, B. Smith, M.C. Monaco, C. Ryschkewitsch, E.O. Major, J. Ohayon, M.K. Schindler, E. Beck, L.B. Recoma, S. Jacobson, D.S. Reich, A. Nath, Pembrolizumab treatmemt for progressive multifocal leukoencephalopathy, N. Engl. J. Med. 380 (2019) 1597–1605.
[72] C. Wang, K.B. Thudium, M. Han, X.-T. Wang, H. Huang, D. Feingersh, C. Garcia, Y. Wu, M. Kuhne, M. Srinivasan, S. Singh, S. Wong, N. Garner, H. Leblanc, R. T. Bunch, D. Blanset, M.J. Selby, A.J. Korman, *In vitro* characterization of the anti-PD-1 antibody nivolumab, BMS-936558, and *in vivo* toxicology in non-human primates, Cancer Immunology Research 2 (2014) 846–856.
[73] A. Worn, A. Pluckthun, Stability engineering of antibody single-chain fv fragments, J. Mol. Biol. 305 (2001) 989–1010.
[74] D.P. Humphreys, O.M. Vetterlein, A.P. Chapman, D.J. King, P. Antoniw, A. J. Suitters, D.G. Reeks, T.A. Parton, L.M. King, B.J. Smith, et al., F(ab')2 molecules made from *Escherichia coli* produced Fab' with hinge sequences conferring increased serum survival in an animal model, J. Immunol. Methods 217 (1998) 1–10.
[75] D.M. Knight, et al., Pharmacodynamic enhancement of the anti-platelet antibody fab abciximab by site-specific pegylation, Platelets 15 (2004) 409–418.
[76] J.L. Casey, R.B. Pedley, D.J. King, A.J. Green, G.T. Yarranton, R.H.J. Begent, Dosimetric evaluation and radioimmunotherapy of anti-tumor multivalent Fab fragments, Br. J. Canc. 81 (1999) 972–980.
[77] P.J. Hudson, C. Souriau, Engineered antibodies, Nat. Med. 9 (2003) 129–134.
[78] P. Bruhns, B. Iannascoli, P. England, D.A. Mancardi, N. Fernandez, S. Jorieux, M. Daeron, Specificity and affinity of human Fc gamma receptors and their polymorphic variants for human IgG subclasses, Blood 113 (2009) 3716–3725.
[79] M. Barok, J. Isola, Z. Palyi-Krekk, P. Nagy, I. Juhasz, G. Vereb, P. Kauraniemi, A. Kapanen, M. Tanner, G. Vereb, J. Szollosi, Trastuzumab causes antibody-dependent cellular cytotoxicity-mediated growth inhibition of submacroscopic JIMT-1 breast cancer xenografts despite intrinsic drug resistance, Moleular Cancer Therapeutics 6 (2019) 2065–2072.
[80] R. Jefferis, Antibody therapeutics: isotype and glycoform selection, Expet Opin. Biol. Ther. 7 (2007) 1401–1413.
[81] G. Scapin, X. Yang, W.W. Prosise, M. McCoy, P. Reichert, J.M. Johnston, R.S. Kashi, C. Strickland, Structure of full-length human anti-PD1 therapeutic IgG4 antibody pembrolizumab, Nature Struct MolBiol 22 (2015) 953–959.
[82] S.P. Arlauckas, C.S. Garris, R.H. Kohler, M. Kitaoka, M.F. Cuccarese, K.S. Yang, M. A. Miller, J.C. Carlson, G.J. Freeman, R.M. Anthony, R. Weissleder, M.J. Pittet, In vivo imaging reveals a tumor-associated macrophage-mediated resistance pathway in anti-PD-1 therapy, Sci. Transl. Med. 9 (2017), eaal3604.
[83] S.L. Topalian, A.H. Sharpe, Balance and imbalance in the immune system: life on the edge, Immunity 41 (2014) 682–684.
[84] H.S. Kuehn, W. Ouyang, B. Lo, E.K. Deenick, J.E. Niemela, D.T. Avery, J.-N. Schickel, D.Q. Tran, J. Stoddard, Y. Zhang, et al., Immune dysregulation in human subjects with heterozygous germline mutations in CTLA4, Science 345 (2014).
[85] J.M. Michot, C. Bigenwald, S. Champiat, M. Collins, F. Carbonnel, S. Postel-Vinay, A. Berdelou, A. Varga, et al., Immune-related adverse events with immune checkpoint blockade: a comprehensive review, Eur. J. Canc. 54 (2016) 139–148.
[86] G.K. Philips, M. Atkins, Therapeutic uses of anti-PD-1 and anti-PD-L1 antibodies, Int. Immunol. 27 (2015) 39–46.
[87] S.L. Topalian, F.S. Hodi, J.R. Brahmer, et al., Safety, activity and immune correlates of anti-PD-1 antibody in cancer, N. Engl. J. Med. 366 (2012) 2443–2454.
[88] J.D. Wolchok, H.M. Kluger, M.K. Callahan, M.A. Postow, N.A. Rizvi, A. M. Lesokhin, N.H. Segal, C.E. Ariyan, R.A. Gordon, K. Reed, et al., Nivolumab plus Ipilmumab in advanced melanoma, N. Engl. J. Med. 369 (2013) 122–133.
[89] B.R. Miller, S.J. Demarest, A. Lugovskoy, F. Huang, X. Wu, W.B. Snyder, L. J. Croner, N. Wang, A. Amatucci, J.S. Michaelson, S.M. Glaser, Stability engineering of scFvs for the development of bispecific and multivalent antibodies, Protein Eng. Des. Sel. 23 (2010) 549–557.
[90] M. Herrmann, C. Krupka, K. Deiser, B. Brauchle, A. Marcinek, A.O. Wagner, F. Rataj, R. Mocikat, K.H. Metzeler, K. Spiekermann, S. Kobold, N.C. Fenn, K. P. Hopfner, M. Subklewe, Bifunctional PD-1 X alphaCD3 X alphaCD33 fusion protein reverses adaptive immune escape in acute myeloid leukemia, Blood 132 (2018) 2484–2494.
[91] W. Meng, A. Tang, X. Ye, X. Gui, L. Li, X. Fan, R.D. Schultz, D.C. Freed, S. Ha, D. Wang, N. Zhang, T.M. Fu, Z. An, Targeting human-cytomegalovirus-infected cells by redirecting T cells using an anti-CD3/anti-glycoproteing B bispecific antibody, Antimicrob. Agents Chemother. 62 (2018) e01719-01717.
[92] E.K. Nyakatura, A.Y. Soare, J.R. Lai, Bispecific antibodies for viral immunotherapy, Hum. Vaccines Immunother. 13 (2017) 836–842.
[93] J. Kaiser, Designer antibodies fight cancer by tethering immune cells to tumor cells, Science 368 (2020) 930–933.
[94] A.N. Niemeijer, D. Leung, M.C. Huisman, I. Bahce, O.S. Hoekstra, G.A.M.S. van Dongen, R. Boellaard, S. Du, W. Hayes, R. Smith, A.D. Windhorst, N.H. Hendrikse, A. Poot, D.J. Vugts, E. Thunnissen, P. Morin, D. Lipovsek, D.J. Donnelly, S. J. Bonacorsi, L.M. Velasquez, T.D. de Gruijl, E.F. Smit, A.J. De Langen, Whole body PD-1 and PD-L1 positron emission tomography in patients with non-small-cell lung cancer, 1038, Nat. Commun. 10 (2018). s41467-41018.
[95] Sanches-Garcia, Recombinant pharmaceuticals from microbial cells, Microbial Cell 15 (2016) 33–37.
[96] L. Lin, L. Li, C. Zhou, J. Li, J. Liu, R. Shu, B. Dong, Q. Li, Z. Wang, A HER2 bispecific antibody can be efficiently expressed in Escherichia coli with potent cytotoxicity, Oncology letters 16 (2018) 1259–1266.
[97] K. Proba, A. Honegger, A. Pluckthun, A natural antibody missing a cysteine in VH: consequences for thermodynamic stability and folding, J. Mol. Biol. 265 (1997) 161–172.